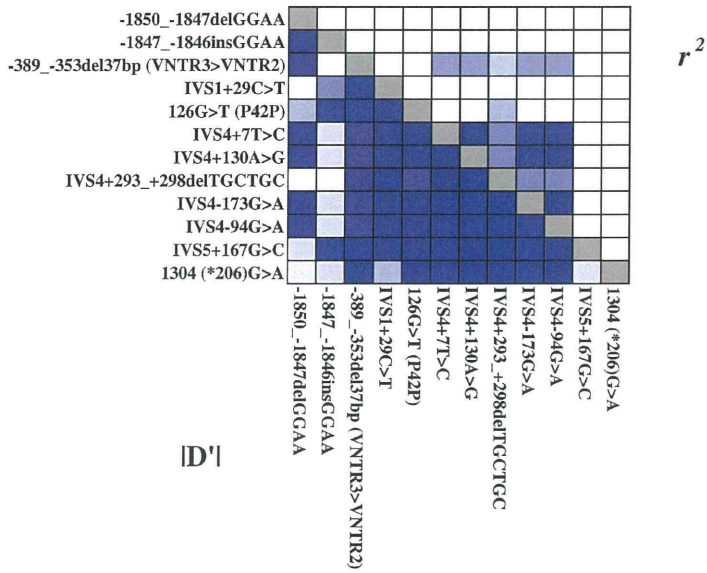

Fig. 1. Linkage disequilibrium (LD) analysis of *FCGRT*
Pairwise LD is expressed as r^2 (upper right) and |D'| (lower left) values (from 0 to 1) by 10-graded blue colors. A denser color represents closer linkage.

($p \geq 0.05$). Two novel non-synonymous variations, 629G > A (R210Q) and 889T > A (S297T), were found as heterozygotes. The allele frequencies were 0.004 for R210Q and 0.020 for S297T. The functional significance of these non-synonymous variations was explored *in vitro* in the following sections. The other coding variations were previously reported synonymous variations. A variable number of tandem repeats (VNTR) was detected in the 5′-flanking region as was found in Caucasian subjects,[8] and the frequencies of VNTR3 (with 3 repeats) and VNTR2 were 0.968 and 0.032, respectively. A short tandem repeat of GGAA was also detected in the 5′-flanking region with a repeat number of 8 (frequency: 0.024), 9 (0.103), 10 (0.754), 11 (0.099) and 12 (0.020). With the 12 detected variations with ≥ 0.03 frequencies, linkage disequilibrium (LD) was analyzed using |D′| and r^2 values (**Fig. 1**). Because of relatively weak linkage between the variations in r^2 values, haplotype analysis was not performed.

Intracellular localization of FcRn variants: Two novel non-synonymous variations, R210Q and S297T, were functionally tested using a mammalian expression system. First, relative expression levels of wild-type and variant FcRn proteins were evaluated by Western blotting. As shown in **Figure 2**, similar levels of the proteins were detected in the three FcRn constructs, and we did not find any statistically significant differences ($p > 0.05$) between the wild-type and the two variants assessed by Dunnett's multiple comparison test when normalized by the expression levels of glyceraldehyde-3-phosphate dehydrogenase as a control. When the wild-type levels were set as 100%, R210Q and S297T levels were 95.08 ± 12.38% and 93.94 ± 13.24%, respectively.

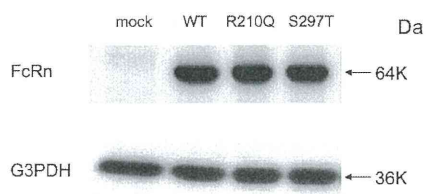

Fig. 2. Western blotting of wild-type and variant FcRns
Cell lysates obtained from the HeLa cells transfected with wild-type or either of the two variant FcRn-EGFP plasmids were subjected to electrophoresis, followed by transfer to the membrane. Detection of FcRn-EGFP was performed as described in Materials and Methods. One representative data of three independent transfections is shown. The FcRn band (64 KDa) consists of 37 KDa of FcRn and 27 KDa of EGFP. Glyceraldehyde-3-phosphate dehydrogenase (G3PDH) levels were used for normalization of the lysate proteins applied to electrophoretic gels.

In order to examine the differences of intracellular localization between wild-type FcRn and its variants, each EGFP fusion construct together with a human β2m construct was transfected into HeLa cells, and fluorescent images were observed by confocal microscopy. There have been several studies reporting the intracellular localization or trafficking of FcRn using fluorescent protein-tagged FcRn.[9–12] N- and C-terminally tagged FcRn showed similar localization.[13] Since FcRn is a type I membrane protein, N-terminal amino acid residues including R210 and S297 were located in the extracellular

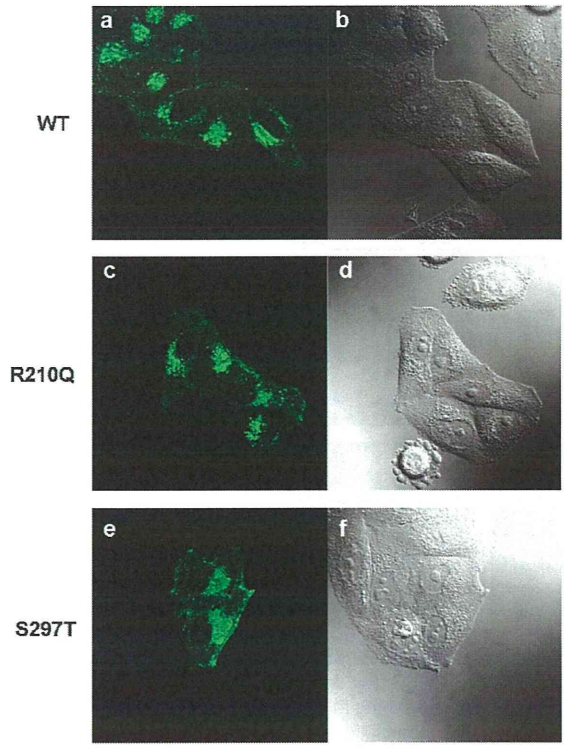

Fig. 3. Intracellular localization of wild-type (WT) and variant FcRns in HeLa cells
HeLa cells were transfected with wild-type (a) or variant (c; R210Q, e; S297T) FcRn-EGFP. The intracellular localization of FcRn-EGFP was observed by confocal laser scanning fluorescence microscopy. Differential interference contrast images of the field are also shown (b, d, f).

or intraluminal region. Therefore, we chose a C-terminal EGFP tag located in the cytoplasmic region of FcRn in order to minimize the effect of the fluorescent tag on the structural environment around the mutation sites.

As shown in **Figure 3a**, the fluorescent signal of wild-type FcRn-EGFP was located primarily in intracellular vesicular components, especially in the perinuclear region. Similar localization was observed for R210Q and S297T variants (**Figs. 3c** and **3e**), suggesting that these amino acid mutations do not affect the intracellular localization of FcRn.

Intracellular co-localization of FcRn variants and incorporated antibody: We then examined the co-localization of the incorporated CypHer5-labeled infliximab and FcRn-EGFP. The binding of CypHer5-labeled infliximab to FcRn was confirmed beforehand (data not shown).

As shown in **Figure 4**, co-localization of FcRn-EGFP and CypHer5-labeled infliximab in intracellular vesicular compartments was observed in HeLa cells expressing wild-type or variant FcRn. Since the fluorescence intensity of CypHer5 increases in acidic pH,[14] the observed fluorescent signal can indicate that CypHer5-labeled infliximab is localized in intracellular acidic compartments such as endosomes. Since the fluorescent images were obtained by confocal microscopy from cells which were washed with neutral pH media, the fluorescence is thought to be derived from incorporated antibodies and not from cell surface-bound antibodies. Therefore, these results showed that both types of FcRn variant, as well as wild-type FcRn, were in acidic endosomes in which incorporated antibodies localized.

Antibody recycling activity of FcRn variants: In order to elucidate the antibody recycling activity of wild-type and variant FcRn, we established the ELISA for biotinylated antibody (infliximab in this study), and measured the amount of recycled antibody from wild-type or variant FcRn-transfected cells. The binding of biotinylated infliximab to FcRn was confirmed by surface plasmon resonance (SPR) analysis (data not shown).

As shown in **Figure 5b**, recycled biotinylated infliximab was detected when the biotinylated infliximab had been loaded to the HeLa cells transfected with wild-type FcRn. The recycling was not detected in mock-transfected cells (**Fig. 5a**), showing that recycling was dependent on expression of FcRn. When the cells were incubated at 4°C for incorporation or recycling, the antibody was not detected in the supernatant. Therefore, recycling was mediated by intracellular trafficking of antibody and not by nonspecific mechanisms. As shown in **Figures 5c** and **5d**, similar levels of antibody recycling were also observed in HeLa cells transfected with either variant FcRn, suggesting similar IgG binding and intracellular trafficking properties of variant FcRns to those of wild-type FcRn. **Figure 6** shows the time course of antibody recycling from cells transfected with wild-type or variant FcRn. The amount of incorporated antibody was measured using the cell lysate at 0 min, and it is noteworthy that no statistical differences assessed by Dunnett's multiple comparison test were observed in the amount of incorporated antibodies between wild-type and either variant FcRn at time 0 (data not shown). The amount of recycled antibody at each time point was expressed as a percentage of the initially incorporated antibody. There was no significant difference between wild-type and the variant FcRns in the amount of recycled antibody, suggesting that these amino acid substitutions do not affect the antibody recycling activity of FcRn.

Discussion

In general, antibody therapeutics have longer half-lives than those of chemical drugs, and the $T_{1/2}$ of IgGs, except for IgG3, in humans is around 21 days. IgG1, IgG2 and IgG4, which are currently used isoforms for antibody therapeutics, have high affinities for FcRn.[15] Escaping from intracellular degradation by binding to FcRn has shown to contribute to this long half-life of the IgGs.

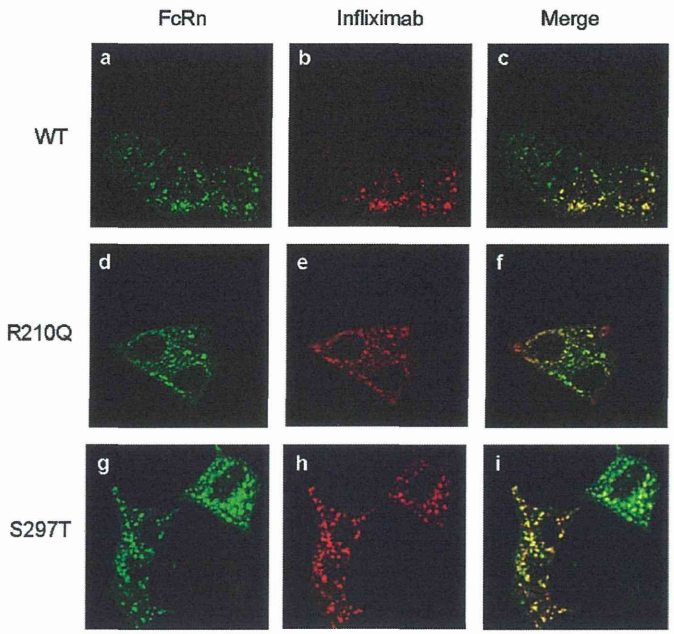

Fig. 4. Co-localization of CypHer5-labeled infliximab and FcRn in HeLa cells expressing wild-type (WT) or a variant FcRn
HeLa cells transfected with wild-type (a, b, c), or variant (d, e, f; R210Q, g, h, i; S297T) FcRn-EGFP were incubated with CypHer5-labeled infliximab in cell culture media containing sodium phosphate buffer (pH. 6.0) for 2–3 hr. After washing the cells twice with neutral pH medium, the fluorescent signal was observed. Panels (a, d, g) and (b, e, h) show the intracellular localization of FcRn-EGFP and the incorporated CypHer5-labeled infliximab, respectively. In panels (c, f, i) the fluorescent signal of FcRn-EGFP was merged with that of CypHer5-labeled infliximab.

Large interindividual variations in pharmacokinetic parameters have been reported for at least several antibody therapeutics. For example, trough concentrations in repetitive dosing of antibodies were reported to show 5.6-fold interindividual differences in 22 palivizumab-treated patients,[16] 18.2-fold differences in 16 cetuximab-treated patients,[17] and over 70-fold differences in 86 infliximab-treated patients.[18] In addition, large percent coefficients of variation were reported for $T_{1/2}$, such as 72.0% for gemtuzumab ozogamicin[19] and 76.4% for basiliximab,[20] after second dose of their treatments. We presumed that changes in FcRn expression levels and function caused by genetic variations of *FCGRT* may lead to these interindividual differences in pharmacokinetics of antibody therapeutics.

In order to identify genetic polymorphisms of *FCGRT*, we sequenced genomic DNA from 126 Japanese subjects. A total of 33 genetic variations, including 17 novel ones, were detected. A VNTR was detected in the 5′ -flanking region, as was the case in Caucasian subjects reported previously.[8] Although a recent study showed that no significant impact was observed in the rates of maternal-fetal IgG transfer,[21] VNTR3 is known to be associated with 1.66-fold higher transcriptional activity than VNTR2 *in vitro*. In addition, monocytes with VNTR3/3 showed increased binding of IgG compared to those with 2/3.[8] Thus, this variation may contribute to the interindividual differences in pharmacokinetics of antibody therapeutics. The allele frequency of VNTR2 in Japanese (0.032) was lower than that in Caucasians (0.075).[8]

In this study, two novel nonsynonymous variations were found and their functional significance was assessed *in vitro* using a mammalian expression system. However, the two FcRn variants did not show any changes in intracellular localization or recycling, suggesting that the two nonsynonymous substitutions found in a Japanese population probably do not contribute to the interindividual variations in the pharmacokinetics of antibody therapeutics. Since FcRn function is important for maintenance of IgG levels as well as maternal-fetal IgG transfer, functionally-affecting genetic variations might be few to retain its functional capability.

Amino acid residues of human FcRn that interact with IgG were reported to be E138, E139, D153 and W154, in the α2 domain.[1] (Amino acid numbers shown in this paper include the signal peptide.). The electrostatic binding of these anionic amino acid residues in FcRn with H310 and H435 in IgG, which has an isoelectric point of pH 7.6, defines the strict pH-dependent binding of IgG to FcRn.[22] The variant amino acid residues identified in this study, R210Q and S297T, are both located in the α3 domain of FcRn. According to the predicted higher order structure,[1] R210 and S297 are located very close to the

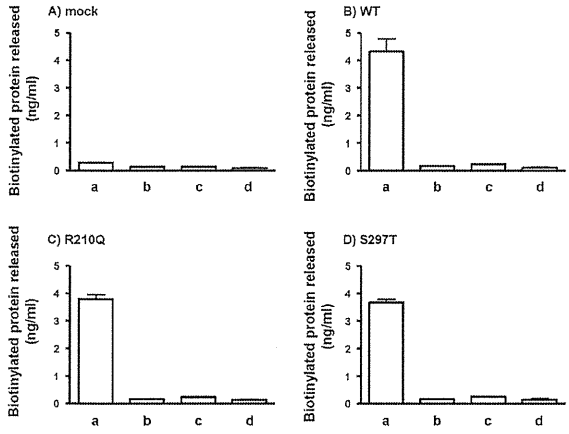

Column	a	b	c	d
Reagents	Infliximab			IgY
Loading Temp. (°C)	37	4	37	37
Recycling Temp. (°C)	37	37	4	37

Fig. 5. Recycling of biotinylated antibodies from wild-type (WT) or variant FcRn-transfected HeLa cells

HeLa cells transfected with wild-type or a variant FcRn were incubated for 1 hr with biotinylated infliximab. After washing, the cells were further incubated for 2 hr. The amount of recycled protein in the supernatant was determined by ELISA. Experimental conditions are shown in the table. For the samples shown as columns a-c, biotinylated infliximab was loaded, whereas biotinylated IgY was used for d. The temperature for antibody loading was 37°C (a, c, d) or 4°C (b). The temperature for recycling antibodies from antibody-loaded cells was 37°C (a, b, d) or 4°C (c).

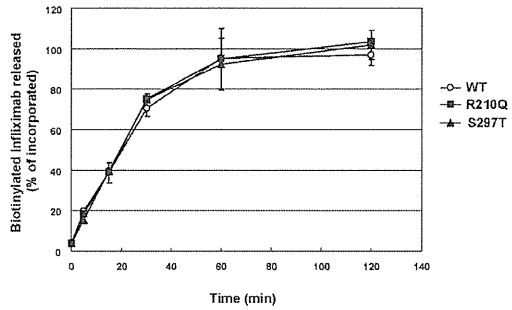

Fig. 6. Quantitative analyses of recycling of biotinylated infliximab; Time course of release of the biotinylated infliximab incorporated into the HeLa cells transfected with wild-type (WT) or variant FcRn

HeLa cells transfected with wild-type or a variant FcRn were incubated for 1 hr with biotinylated infliximab. After washing, cells were further incubated for the indicated periods of time. The amount of recycled protein was determined by ELISA. The amount of recycled antibody at each time point was expressed as a percentage of the initially incorporated antibody at time 0.

transmembrane region that is distant from the IgG binding site. Considering the results obtained here, where no difference in antibody recycling activity between wild-type and each variant FcRn was detected *in vitro*, the amino acid substitutions identified in a Japanese population may not have significant impact on structural and functional properties of FcRn. Although FcRn is known to bind with albumin as well as IgG, the albumin binding site of FcRn has been identified as H189, which also is located in the α2 domain.[23] The polymorphic sites are also far from the albumin binding site. However, the effect of amino acid substitutions R210Q and S297T on the albumin recycling activity via FcRn should be determined in a future study.

In the present study, we used HeLa cells to examine the localization and recycling activity of FcRn variants. Since endogenous expression of FcRn protein in HeLa cells has not been detected,[24] we considered HeLa cells suitable for examining the antibody recycling activity of variant FcRn since the background responses are negligible. In fact, as shown in **Figure 5**, antibody recycling was detected only in FcRn-transfected cells. Therefore, we concluded that HeLa cells can be used as a suitable model for evaluating the function of variant FcRn proteins.

Our results suggested that at least no common functional polymorphic site with amino acid change was present in *FCGRT* in our Japanese population. Since FcRn function is important for maintenance of IgG levels, there may be few functionally-affecting genetic variations. Further analysis is necessary for the functional significance of transcriptional regulatory regions.

Acknowledgement: We thank Ms. Chie Sudo for secretarial assistance.

References

1) Andersen, J. T. and Sandlie, I.: The versatile MHC class I-related FcRn protects IgG and albumin from degradation: implications for development of new diagnostics and therapeutics. *Drug Metab. Pharmacokinet.*, **24**: 318–332 (2009).
2) Lobo, E. D., Hansen, R. J. and Balthasar, J. P.: Antibody pharmacokinetics and pharmacodynamics. *J. Pharm. Sci.*, **93**: 2645–2668 (2004).
3) Suzuki, T., Ishii-Watabe, A., Tada, M., Kobayashi, T., Kanayasu-Toyoda, T., Kawanishi, T. and Yamaguchi, T.: Importance of neonatal FcR in regulating the serum half-life of therapeutic proteins containing the Fc domain of human IgG1: a comparative study of the affinity of monoclonal antibodies and Fc-fusion proteins to human neonatal FcR. *J. Immunol.*, **184**: 1968–1976 (2010).
4) Claypool, S. M., Dickinson, B. L., Yoshida, M., Lencer, W. I. and Blumberg, R. S.: Functional reconstitution of human FcRn in Madin-Darby canine kidney cells requires co-expressed human beta 2-microglobulin. *J. Biol. Chem.*, **277**: 28038–28050 (2002).
5) Praetor, A. and Hunziker, W.: Beta(2)-microglobulin is important for cell surface expression and pH-dependent IgG bind-

ing of human FcRn. *J. Cell. Sci.*, **115**: 2389–2397 (2002).
6) Tesar, D. B., Tiangco, N. E. and Bjorkman, P. J.: Ligand valency affects transcytosis, recycling and intracellular trafficking mediated by the neonatal Fc receptor. *Traffic*, **7**: 1127–1142 (2006).
7) Kamei, D. T., Lao, B. J., Ricci, M. S., Deshpande, R., Xu, H., Tidor, B. and Lauffenburger, D. A.: Quantitative methods for developing Fc mutants with extended half-lives. *Biotechnol. Bioeng.*, **92**: 748–760 (2005).
8) Sachs, U. J., Socher, I., Braeunlich, C. G., Kroll, H., Bein, G. and Santoso, S.: A variable number of tandem repeats polymorphism influences the transcriptional activity of the neonatal Fc receptor alpha-chain promoter. *Immunology*, **119**: 83–89 (2006).
9) Goebl, N. A., Babbey, C. M., Datta-Mannan, A., Witcher, D. R., Wroblewski, V. J. and Dunn, K. W.: Neonatal Fc receptor mediates internalization of Fc in transfected human endothelial cells. *Mol. Biol. Cell.*, **19**: 5490–5505 (2008).
10) Ober, R. J., Martinez, C., Lai, X., Zhou, J. and Ward, E. S.: Exocytosis of IgG as mediated by the receptor, FcRn: an analysis at the single-molecule level. *Proc. Natl. Acad. Sci. U.S.A.*, **101**: 11076–11081 (2004).
11) Ober, R. J., Martinez, C., Vaccaro, C., Zhou, J. and Ward, E. S.: Visualizing the site and dynamics of IgG salvage by the MHC class I-related receptor, FcRn. *J. Immunol.*, **172**: 2021–2029 (2004).
12) Ward, E. S., Martinez, C., Vaccaro, C., Zhou, J., Tang, Q. and Ober, R. J.: From sorting endosomes to exocytosis: association of Rab4 and Rab11 GTPases with the Fc receptor, FcRn, during recycling. *Mol. Biol. Cell.*, **16**: 2028–2038 (2005).
13) Gan, Z., Ram, S., Vaccaro, C., Ober, R. J. and Ward, E. S.: Analyses of the recycling receptor, FcRn, in live cells reveal novel pathways for lysosomal delivery. *Traffic*, **10**: 600–614 (2009).
14) Mark, S. B., Burns, D. D., Cooper, M. E. and Gregory, S. J.: A pH sensitive fluorescent cyanine dye for biological applications. *Chem. Commun.*, **23**: 2323–2324 (2000).
15) Ternant, D. and Paintaud, G.: Pharmacokinetics and concentration-effect relationships of therapeutic monoclonal antibodies and fusion proteins. *Expert Opin. Biol. Ther.*, **5 Suppl 1**: S37–47 (2005).
16) Subramanian, K. N., Weisman, L. E., Rhodes, T., Ariagno, R., Sanchez, P. J., Steichen, J., Givner, L. B., Jennings, T. L., Top, F. H. Jr, Carlin, D. and Connor, E.: Safety, tolerance and pharmacokinetics of a humanized monoclonal antibody to respiratory syncytial virus in premature infants and infants with bronchopulmonary dysplasia. MEDI-493 Study Group. *Pediatr. Infect. Dis. J.*, **17**: 110–115 (1998).
17) Cézé, N., Ternant, D., Piller, F., Degenne, D., Azzopardi, N., Dorval, E., Watier, H., Lecomte, T. and Paintaud, G.: An enzyme-linked immunosorbent assay for therapeutic drug monitoring of cetuximab. *Ther. Drug Monit.*, **31**: 597–601 (2009).
18) St Clair, E. W., Wagner, C. L., Fasanmade, A. A., Wang, B., Schaible, T., Kavanaugh, A. and Keystone, E. C.: The relationship of serum infliximab concentrations to clinical improvement in rheumatoid arthritis: results from ATTRACT, a multicenter, randomized, double-blind, placebo-controlled trial. *Arthritis Rheum.*, **46**: 1451–1459 (2002).
19) Dowell, J. A., Korth-Bradley, J., Liu, H., King, S. P. and Berger, M. S.: Pharmacokinetics of gemtuzumab ozogamicin, an antibody-targeted chemotherapy agent for the treatment of patients with acute myeloid leukemia in first relapse. *J. Clin. Pharmacol.*, **41**: 1206–1214 (2001).
20) Kovarik, J. M., Nashan, B., Neuhaus, P., Clavien, P. A., Gerbeau, C., Hall, M. L. and Korn, A.: A population pharmacokinetic screen to identify demographic-clinical covariates of basiliximab in liver transplantation. *Clin. Pharmacol. Ther.*, **69**: 201–209 (2001).
21) Freiberger, T., Ravcuková, B., Grodecká, L., Kurecová, B., Jarkovský, J., Bartonková, D., Thon, V. and Litzman, J.: No association of FCRN promoter VNTR polymorphism with the rate of maternal-fetal IgG transfer. *J. Reprod. Immunol.*, **85**: 193–197 (2010).
22) Vaughn, D. E., Milburn, C. M., Penny, D. M., Martin, W. L., Johnson, J. L. and Bjorkman, P. J.: Identification of critical IgG binding epitopes on the neonatal Fc receptor. *J. Mol. Biol.*, **274**: 597–607 (1997).
23) West, A. P., Jr. and Bjorkman, P. J.: Crystal structure and immunoglobulin G binding properties of the human major histocompatibility complex-related Fc receptor. *Biochemistry*, **39**: 9698–9708 (2000).
24) Liu, X., Ye, L., Christianson, G. J., Yang, J. Q., Roopenian, D. C. and Zhu, X.: NF-kappaB signaling regulates functional expression of the MHC class I-related neonatal Fc receptor for IgG via intronic binding sequences. *J. Immunol.*, **179**: 2999–3011 (2007).

Science Translational Medicine
AAAS

Improving Drug Potency and Efficacy by Nanocarrier-Mediated Subcellular Targeting

Mami Murakami, *et al.*

Sci Transl Med **3**, 64ra2 (2011);
DOI: 10.1126/scitranslmed.3001385

RESEARCH ARTICLE

DRUG DELIVERY

Improving Drug Potency and Efficacy by Nanocarrier-Mediated Subcellular Targeting

Mami Murakami,[1] Horacio Cabral,[1,2] Yu Matsumoto,[3] Shourong Wu,[3] Mitsunobu R. Kano,[4] Takao Yamori,[5] Nobuhiro Nishiyama,[2,3]* Kazunori Kataoka[1,2,3,6]*

Nanocarrier-mediated drug targeting is an emerging strategy for cancer therapy and is being used, for example, with chemotherapeutic agents for ovarian cancer. Nanocarriers are selectively accumulated in tumors as a result of their enhanced permeability and retention of macromolecules, thereby enhancing the antitumor activity of the nanocarrier-associated drugs. We investigated the real-time subcellular fate of polymeric micelles incorporating (1,2-diaminocyclohexane) platinum(II) (DACHPt/m), the parent complex of oxaliplatin, in tumor tissues by fluorescence-based assessment of their kinetic stability. These observations revealed that DACHPt/m was extravasated from blood vessels to the tumor tissue and dissociated inside each cell. Furthermore, DACHPt/m selectively dissociated within late endosomes, enhancing drug delivery to the nearby nucleus relative to free oxaliplatin, likely by circumvention of the cytoplasmic detoxification systems such as metallothionein and methionine synthase. Thus, these drug-loaded micelles exhibited higher antitumor activity than did oxaliplatin alone, even against oxaliplatin-resistant tumors. These findings suggest that nanocarriers targeting subcellular compartments may have considerable benefits in clinical applications.

INTRODUCTION

In 2009, about 10 million people worldwide were newly diagnosed with cancer (*1*). Application of nanotechnology to cancer therapy may offer therapeutic effects that cannot be achieved with other strategies. The main aim of this approach is to develop nanoscale drug vehicles for targeted cancer therapy (*2*–*5*). Nanocarriers selectively accumulate in solid tumors as a result of the enhanced permeability and retention (EPR) effect, which is characterized by microvascular hyperpermeability to circulating macromolecules and impaired lymphatic drainage in tumor tissues (*6*). At present, several nanocarrier formulations have been approved for clinical use against ovarian cancer and HIV-associated Kaposi's sarcoma (Doxil) and breast cancer (Abraxane). These formulations allow better accumulation of the drugs doxorubicin and paclitaxel in tumors (*7*).

Polymeric micelles, self-assemblies of block copolymers, have gained increasing popularity as tumor-targetable nanocarriers since they were first used as drug vehicles in the late 1980s (*8*–*12*). These micelles, which are several tens of nanometers in size and have a characteristic core-shell structure consisting of a drug-loaded hydrophobic core and poly(ethylene glycol) (PEG) hydrophilic shell, are long-lived in the bloodstream and effectively accumulate in solid tumors after intravenous injection (*8*). The critical features of polymeric micelles for their function as drug vehicles, including size, drug loading and release, and specific binding to the target cells, can be modulated by engineering the constituent block copolymers. At present, our micelle formulations incorporating doxorubicin, paclitaxel, SN-38, cisplatin, and (1,2-diaminocyclohexane) platinum(II) (DACHPt) are undergoing clinical trials (development code names NK911, NK105, NK012, NC-6004, and NC-4016, respectively), and four of these have advanced to Phase II studies (*13*–*17*). These clinical studies have revealed that polymeric micelles reduce side effects from the incorporated drugs and are effective against various intractable tumors, such as triple-negative breast cancers (*18*), indicating their clinical potential.

Recently, increasing attention has been paid to another potentially useful property of nanocarriers: to achieve subcellular drug targeting. Subcellular drug targeting of nanocarriers could enhance the pharmacological activity of the loaded drugs through improved subcellular drug distribution (*19*). Drug vehicles designed to release active drugs in acidic organelles, such as the endosome and lysosome, can circumvent recognition by the drug efflux pump (for example, P-glycoprotein) through internalization by endocytosis, thus overcoming multidrug resistance in cancer cells (*20*–*22*). Here, we aimed to investigate the potential of DACHPt-loaded micelles (DACHPt/m) for in vivo subcellular targeting. DACHPt/m is formed by the polymer-metal complexation between DACHPt and the carboxylic group of poly(ethylene glycol)-*b*-poly(glutamic acid) [PEG-*b*-P(Glu)] copolymers. DACHPt is the parent complex of the clinically approved drug oxaliplatin. Oxaliplatin has a hydrolyzable oxalate group to increase its solubility in water, which can be removed by nucleophiles in biological media, such as chloride ions. Aqua complexes ($[(DACH)Pt(H_2O)Cl]^+$ or $[(DACH)Pt(H_2O)_2]^{2+}$) of DACHPt exhibit chemotherapeutic activity. DACHPt/m releases DACHPt and the micelle structure dissociates depending on the pH and chloride ion concentrations, a result of ligand substitution of the Pt(II) from the carboxylates in the micelle core with the chloride ions in the medium (Fig. 1A) (*23*, *24*). Moreover, after DACHPt/m is internalized into cancer cells, it would be expected to be exposed to different pH and chloride ion concentrations during subcellular trafficking (*25*). We hypothesized that DACHPt/m would be selectively released in low-pH cellular compartments, bypassing

[1]Department of Bioengineering, Graduate School of Engineering, University of Tokyo, 7-3-1 Hongo, Bunkyo-ku, Tokyo 113-8656, Japan. [2]Center for NanoBio Integration, University of Tokyo, Tokyo 113-8656, Japan. [3]Center for Disease Biology and Integrative Medicine, Graduate School of Medicine, University of Tokyo, Tokyo 113-0033, Japan. [4]Department of Molecular Pathology, Graduate School of Medicine, University of Tokyo, Tokyo 113-0033, Japan. [5]Division of Molecular Pharmacology, Cancer Chemotherapy Center, Japanese Foundation for Cancer Research, 3-10-6 Ariake, Koto-ku, Tokyo 135-8550, Japan. [6]Department of Materials Engineering, Graduate School of Engineering, University of Tokyo, Tokyo 113-8656, Japan.
*To whom correspondence should be addressed. E-mail: nishiyama@bmw.t.u-tokyo.ac.jp (N.N.); kataoka@bmw.t.u-tokyo.ac.jp (K.K.)

cytoplasmic detoxification and thereby improving potency and efficacy (Fig. 1B). Indeed, we previously reported that cisplatin-loaded micelles, which are formed in the same manner as DACHPt/m, caused different gene expression patterns than did cisplatin alone because of their different internalization pathways and the facilitated drug release in endosomes and lysosomes (*26*). To test the above-mentioned hypothesis, we constructed fluorescent-labeled DACHPt/m (F-DACHPt/m) with a dual fluorescent-labeling method so that we could follow the intracellular localization and dissociation of the micelles by using in vivo confocal microscopy, and intravitally evaluated the extravasation, penetration, cellular uptake, and subcellular fate of DACHPt/m in tumor tissues and their activity against human colorectal cancers.

RESULTS

Construction and characterization of F-DACHPt/m

To construct the dual fluorescent-labeled block copolymer, we conjugated the fluorescent dyes boron dipyrromethene (BODIPY) FL (excitation wavelength, 503 nm; emission wavelength, 512 nm) and BODIPY TR (excitation wavelength, 588 nm; emission wavelength, 616 nm) to the α- and ω-end groups of α-4-(diethoxymethyl)benzyl-poly(ethylene glycol)-*b*-poly(L-glutamic acid), respectively, and thus obtained BODIPY FL-PEG-*b*-P(Glu)-BODIPY TR (fig. S1). The conjugation degree for BODIPY FL to the block copolymer was 0.2 mol BODIPY FL per mole of polymer and for BODIPY TR was about 0.8 mol BODIPY TR per mole of polymer. We built F-DACHPt/m by the formation of polymer-metal complexes between DACHPt and the carboxylic groups of poly(glutamic acid) in BODIPY FL-PEG-*b*-P(Glu)-BODIPY TR (Fig. 1A). F-DACHPt/m had a diameter of 30 nm, similar to that of DACHPt/m (fig. S2). The intact F-DACHPt/m emitted fluorescence only from the shell-conjugated dye (BODIPY FL) because the core-conjugated dye (BODIPY TR) was quenched owing to its high local concentration. The close proximity of BODIPY TR fluorophores in the core of the micelles leads to self-quenching by the formation of nonfluorescent ground-state BODIPY TR dimers (or higher aggregates) (*27*). When DACHPt is released as a result of the ligand substitution of the Pt(II) from the carboxylates in the micelle core with the chloride in the medium, the density of the micelle core is reduced and the fluorescence of BODIPY TR is dequenched (Fig. 1A). We investigated the release of DACHPt from F-DACHPt/m and the fluorescence of BODIPY FL and BODIPY TR at the surface and core of the micelles, respectively, under conditions that mimicked the extracellular medium (pH 7.4 and 150 mM Cl^-), early endosomes (pH 6.9 and 20 mM Cl^-), and late endosomes and lysosomes (pH 5.5 and 70 mM Cl^-) (*25*). The fluorescence from BODIPY FL on the shell of the micelles was constant regardless of the pH and salt concentration of the media (Fig. 2, A to C, middle columns), suggesting that the fluorescence from BODIPY FL can be used to trace the position of the micelles in the biological environment. In addition, the drug release profile of F-DACHPt/m was similar to that of unmodified DACHPt/m, suggesting the feasibility of a direct comparison (Fig. 2, A to C, left columns). Under extracellular conditions, BODIPY TR fluorescence increased after an incubation period of 17 hours, simultaneous with the release of DACHPt from F-DACHPt/m (Fig. 2A). The release of DACHPt from F-DACHPt/m in the late endosomal conditions was considerably faster (Fig. 2C) than in the extra-

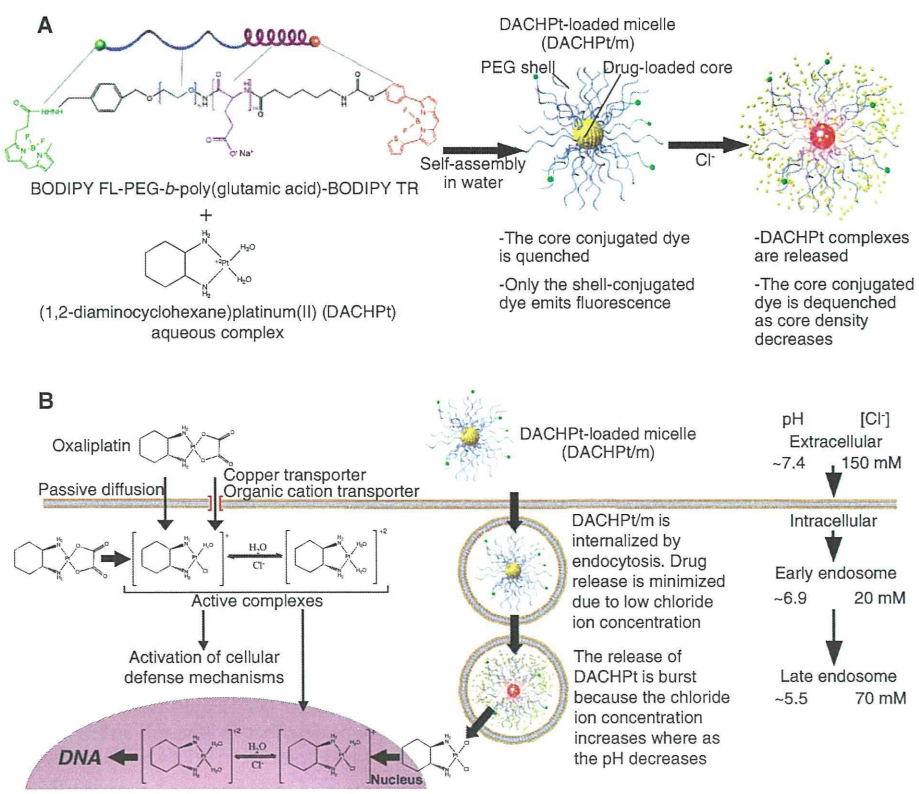

Fig. 1. Design of fluorescent-labeled DACHPt/m (F-DACHPt/m) for visualization of the localization and drug release in the cell. (**A**) F-DACHPt/m self-assembled through polymer-metal complex formation between DACHPt and boron dipyrromethene (BODIPY) FL–poly(ethylene glycol)-*b*-poly(glutamic acid)–BODIPY TR in distilled water. In the micelle state, only BODIPY FL (green) emits fluorescence, whereas BODIPY TR (red) remains quenched. As DACHPt is released from F-DACHPt/m in chloride ion–containing media, BODIPY TR is dequenched and emits fluorescence. (**B**) Schematic representation of hypothetical subcellular pathways and action of DACHPt/m. Oxaliplatin enter cells by passive diffusion or through copper/organic cation transporters. Once oxaliplatin is in the cytoplasm, most of the activated aqua species ($[(DACH)Pt(H_2O)Cl]^+$ or $[(DACH)Pt(H_2O)_2]^{2+}$) are eliminated by cellular detoxification mechanisms, but a small fraction binds to DNA. In contrast, DACHPt/m that enters tumor cells by endocytosis (middle) is exposed to an environment with increasing acidity and chloride ion concentration because early endosomes mature into the late endosomes. Drug release from DACHPt/m is accelerated in the late endosomal environment close to the perinuclear region, resulting in enhanced efficiency of drug delivery to the nucleus.

cellular and early endosomal conditions (Fig. 2, A and B), occurring without any delay. Further, mirroring the DACHPt release, F-DACHPt/m exhibited more robust fluorescence recovery of BODIPY TR under the late endosomal conditions (Fig. 2C) than under the early endosomal conditions (Fig. 2B, right columns). Thus, the fluorescence profiles of BODIPY TR are correlated with the release profiles of DACHPt from the micelles.

In vitro subcellular trafficking of F-DACHPt/m

The cellular internalization and fate of F-DACHPt/m in human tumor-derived colorectal cancer (HT29) cells, which are the most frequently used cell lines in oxaliplatin studies (*28*), were observed with time-lapse confocal laser scanning microscopy (CLSM) (Fig. 3A and video S1). The intensity of BODIPY FL fluorescence increased slightly over time (Fig. 3B), and the BODIPY FL fluorescence in the images was clearly visible within a 6-hour incubation (Fig. 3A). Meanwhile, with time, the intensity of BODIPY TR fluorescence continuously increased to a greater extent than did that of BODIPY FL fluorescence (Fig. 3B), and the BODIPY TR fluorescence in the images became visible at about 24 hours of incubation (Fig. 3A). This continuous increase in the intensity of BODIPY TR fluorescence corresponds to the dequenching of BODIPY TR fluorescence driven by the release of DACHPt in the cell. These results suggest that F-DACHPt/m enters the cells as a micelle form and then dissociates within the subcellular environments.

Using CLSM with higher magnification, we further evaluated the detailed subcellular trafficking and fate of F-DACHPt/m by focusing on individual cells. We confirmed that the micelles entered the cancer cells via endocytosis by incubating the cells with F-DACHPt/m at 37°C and 4°C. As endocytosis ceases at 4°C, the fluorescent signal of F-DACHPt/m inside the cells was undetectable, whereas at 37°C, the fluorescence from F-DACHPt/m was observed inside the cells (fig. S3). To examine the subcellular trafficking of the micelles, we determined the colocalization of BODIPY FL fluorescence from F-DACHPt/m with an early endosome marker, Rab5a-RFP, and a late endosome and lysosome marker, LysoTracker, in HT29 cells (Fig. 3C). Note that individual vesicular organelles can be recognized as punctate fluorescence in the images. After a 6-hour incubation at 37°C, BODIPY FL colocalized mainly with Rab5a-RFP (yellow fluorescence in Fig. 3C, upper images) rather than with LysoTracker. After prolonged incubation (24 and 55 hours), BODIPY FL showed decreased colocalization with Rab5a-RFP and increased colocalization with LysoTracker (yellow fluorescence in Fig. 3C, lower images). This observation was confirmed by quantification of colocalized fluorescent intensities of BODIPY FL with Rab5a-RFP or LysoTracker (Fig. 3D). These results suggested that the micelles might localize mainly in the early endosome until 6 hours and then move into the late endosome/lysosome compartment. Furthermore, we studied the timing and location of the micelle dissociation and concomitant drug release by evaluating the colocalization of F-DACHPt/m with LysoTracker (Fig. 3E and fig. S4A) and the quantification of BODIPY FL and BODIPY TR fluorescent intensities (fig. S4B), as well as the colocalization ratio (Fig. 3F). The fluorescence intensity from BODIPY FL gradually increased (fig. S4B). Meanwhile, the fluorescence of BODIPY TR became visible after 24-hour incubation (Fig. 3E and fig. S4A) and then increased over time (fig. S4B). Both BODIPY FL and BODIPY TR colocalized with LysoTracker (Fig. 3E and fig. S4A), and the colocalization ratio between BODIPY FL or BODIPY TR and LysoTracker increased over time (Fig. 3F). These observations sug-

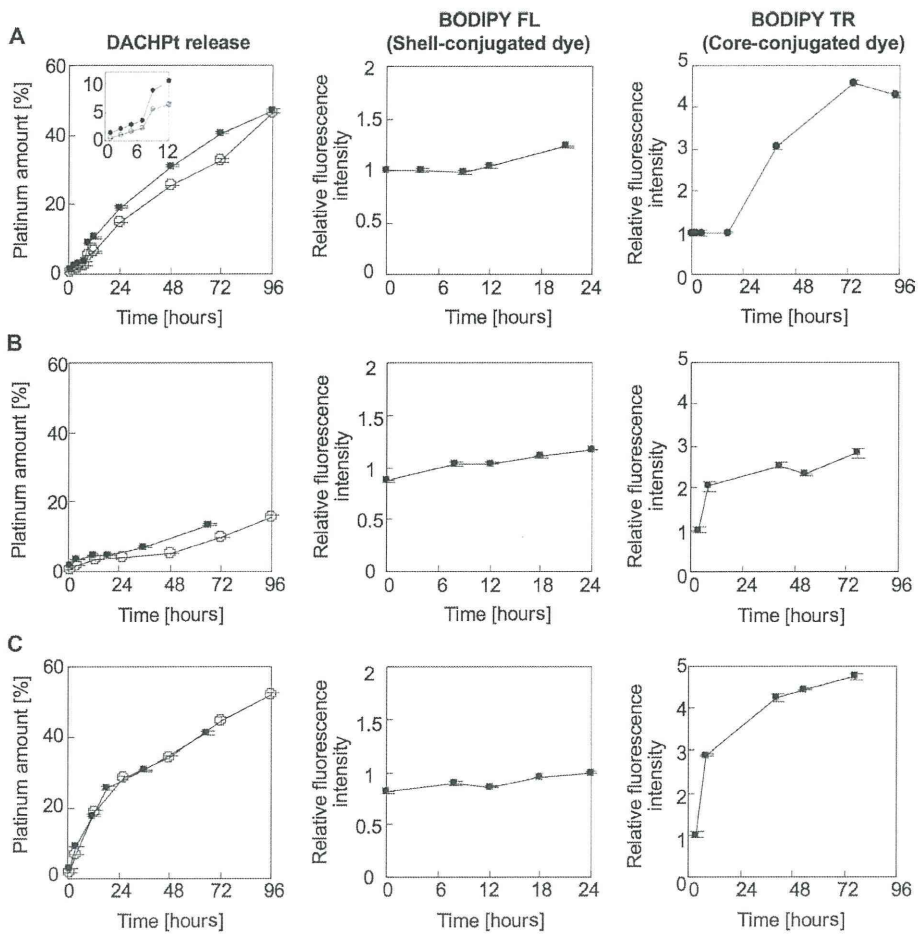

Fig. 2. Properties of F-DACHPt/m under conditions mimicking extracellular and subcellular environments. (**A** to **C**) Release profiles of DACHPt from DACHPt/m and F-DACHPt/m (left column) and fluorescence profiles of BODIPY FL (middle column) and BODIPY TR (right column) under conditions mimicking (A) the extracellular environment (10 mM PBS, pH 7.4, and 150 mM NaCl), (B) the early endosomal environment (10 mM PBS, pH 6.9, and 20 mM NaCl), and (C) the late endosomal environment (10 mM PBS, pH 5.5, and 70 mM NaCl), all at 37°C. Inset in top left panel is the magnification of the profiles of DACHPt release until 12 hours. The release of DACHPt from the micelles was evaluated by dialysis as described in Materials and Methods. Data for DACHPt/m and F-DACHPt/m in the left column are shown as open and filled circles, respectively. Data are expressed as means ± SEM ($n = 3$).

gested that F-DACHPt/m progressively dissociated in the late endosome and lysosomal compartments. Because these acidic organelles reside in the perinuclear region, F-DACHPt/m would be expected to deliver the active platinum complexes close to the nucleus. Thus, in vitro confocal microscopy revealed that F-DACHPt/m appears to exhibit late endosome/lysosome–selective dissociation concomitant with the release of DACHPt, thereby achieving efficient DACHPt delivery close to the nucleus.

Effect of subcellular pathway on drug efficiency

Oxaliplatin enters the cells by passive diffusion or through copper/organic cation transporters (*29*), and it then changes to active DACHPt aqua complexes in the cytoplasm, some of which may ultimately cross-link with DNA, disrupting DNA function and exerting therapeutic activity (Fig. 1B). However, 75 to 85% of activated platinum drugs are sequestered by abundant sulfur species that serve as cellular defense mechanisms in the cytoplasm, and only 5 to 10% of oxaliplatin can bind to DNA (Fig. 1B) (*30*–*32*). We hypothesized that DACHPt/m facilitates drug delivery close to the nucleus through its perinuclear subcellular localization. Therefore, we studied the pharmacological activity of DACHPt/m. DACHPt/m displayed a value of IC_{50} (the mean concentration that causes 50% growth inhibition) against HT29 cells that was lower than that of oxaliplatin by a factor of 4.7 (Table 1). It is rare that a nanocarrier-encapsulated drug surpasses the free form of the drug for in vitro cytotoxicity (*33*). To elucidate the mechanism of DACHPt/m action, we evaluated the subcellular accumulation of platinum and quantity of Pt-DNA adducts. Exposure of HT29 cells to oxaliplatin resulted in twice as much accumulation of platinum than did exposure to DACHPt/m (Fig. 3G). This is probably because oxaliplatin rapidly enters the cells by diffusion and through copper/organic cation transporters (*29*), whereas DACHPt/m is gradually internalized by endocytosis. Nevertheless, we did not observe a significant difference in the Pt-DNA adducts formed after exposure to oxaliplatin and DACHPt/m (Fig. 3H), indicating that DACHPt/m may efficiently deliver the active platinum drug to DNA (Fig. 3I).

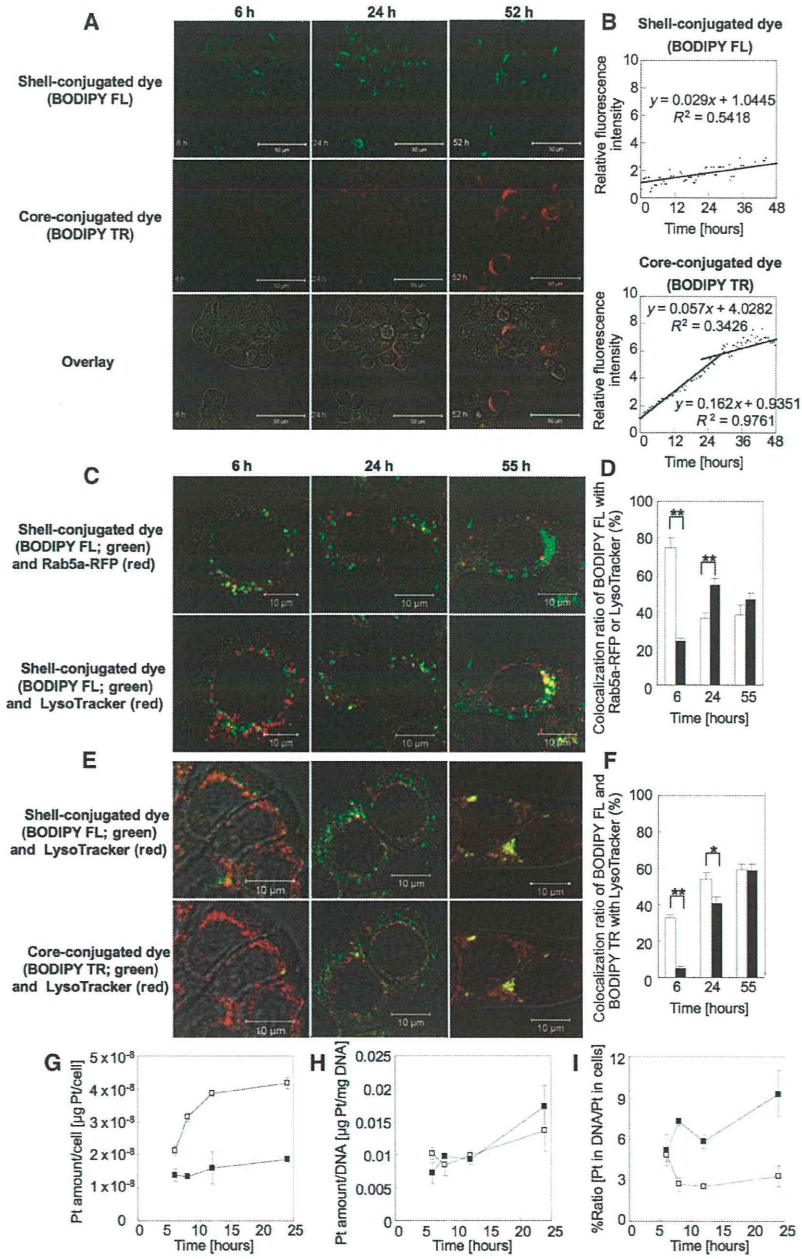

Fig. 3. In vitro observation of subcellular trafficking and fate of F-DACHPt/m, cellular platinum accumulation, and formation of platinum-DNA adducts. (**A**) Representative images of time-lapse CLSM observation of HT29 cells treated with F-DACHPt/m (green, BODIPY FL; red, BODIPY TR; yellow, their colocalization). (**B**) Relative fluorescence intensity of BODIPY FL (upper) and BODIPY TR (lower) of F-DACHPt/m. (**C**) Fluorescent images of colocalization of BODIPY FL of DACHPt/m (green) with an early endosome marker, Rab5a-RFP (red in upper images), or a late endosome and lysosome marker, LysoTracker (red in lower images), in HT29 cells after incubation for 6, 24, and 55 hours. (**D**) Colocalization ratio of BODIPY FL with Rab5a-RFP (open bars) or LysoTracker (closed bars). Data are expressed as means ± SEM ($n = 10$). $^{**}P < 0.01$. (**E**) Fluorescent images of colocalization of BODIPY FL (green in upper images) and BODIPY TR (green in lower images) of F-DACHPt/m with LysoTracker (red) in HT29 cells after incubation for 6, 24, and 55 hours. (**F**) Colocalization ratio of BODIPY FL (open bars) or BODIPY TR (closed bars) with LysoTracker. Data are expressed as means ± SEM ($n = 10$). $^{*}P < 0.05$; $^{**}P < 0.01$. (**G**) In vitro cellular accumulation of platinum. (**H**) DNA platination. (**I**) Ratio of platinum in DNA to total platinum in cells expressed as a percentage. DNA platination was converted from μg Pt/mg DNA to μg Pt/cell, and the ratio was calculated. Open squares, oxaliplatin; filled squares, DACHPt/m. Data are expressed as means ± SEM ($n = 3$).